ORIGINAL SCIENTIFIC PAPER

ACTA GRAPHICA 236

Thermal evolution process, properties and photocatalytic activity of sol-gel derived nanocrystalline anatase in dye degradation process

Authors

Iva Minga, Stanislav Kurajica, Vilko Mandić

Faculty of chemical engineering and technology, University of Zagreb, Croatia
iminga@fkit.hr

Abstract:

Nanocrystalline anatase aimed to be used as a photocatalyst for dye degradation processes in industrial effluents and has been prepared and investigated. Amorphous titania gel has been prepared using sol–gel process by slow hydrolysis of titanium *n*–butoxide. The prepared gel has been investigated using Fourier–Transformed Infra–Red Spectroscopy (FTIR), Powder X–ray Diffraction (PXRD), Differential Thermal Analysis (DTA), Thermo–Gravimetric Analysis (TGA), N_2 gas adsorption–desorption isotherms and Diffuse Reflectance UV–Vis Spectroscopy (DRS).
It was determined that the amorphous gel was comprised of non-hydrolyzed butoxy groups as well as hydroxyl groups bonded to titanium. The thermal evolution of gel is consisted of five steps: elimination of adsorbed water and butanol in temperature range between room temperature and 200 °C, decomposition and elimination of butoxy groups between 200 and 300°C. The crystallization of anatase centered at 404°C, transformation to rutile starting from 540 °C and oxidation of char and tar above 600°C.
Thermal treatment of gel at 350 °C for 2 h yields with pure nanocrystalline anatase with average crystallite size of 13.2±0.2 nm, specific surface area of 65.48 m^2g^{-1} and bandgap, of 3.24 eV. The preliminary assessment of prepared catalyst photocatalytic activity was obtained through degradation process of methylene blue dye under UV light and the 99 % degradation of dye took place within 150 min.

Keywords:

nanocrystalline anatase, sol-gel, photocatalysis, dyes.

1. Introduction

Dyes are commonly used in many industries such as food, paper, textile, rubbers, plastics, cosmetics in order to colour their products. The discharge of coloured wastes into streams affects the aesthetic nature and interferes with the transmission of sunlight into streams reducing photosynthetic activity (Dogan and Alkan, 2003; Mall, Srivastava and Agarwal, 2006). The non-biodegradable nature of dyes and their stability toward light and oxidizing agents complicate the

selection of a suitable method for their removal (Pokhrel and Viraraghavan, 2004).

The traditional techniques for dye removal from wastewater are biological treatment, adsorption and coagulation. Each method has its advantages and disadvantages. Large degree of aromatics present in dye molecules and the stability of modern dyes make conventional biological decolorization and degradation treatment methods ineffective for (Lachheb, et al., 2002). Adsorption is nondestructive method, since it just transfers dyes from water to another phase, thus causing secondary pollution. Consequently, regeneration of the adsorbent materials and post-treatment of solid-wastes, which are expensive operations, are needed. Coagulation, using alums, ferric salts, or limes is low-cost process but it suffers from the waste disposal problem.

Over the last two decades, photocatalysis has been shown to be potentially advantageous and useful for the degradation of wastewater pollutants (Sivalingam, et al., 2003). Several advantages of this process are: complete mineralization of organic pollutants to CO_2, water and mineral acids, no waste-solids disposal problem, and only mild temperature and pressure conditions are necessary. Nanocrystalline titania powders have been widely studied with respect to potential photocatalytic, photovoltaic and optical applications (Chen and Mao, 2007; Li, et al., 2009; Sugimoto, Zhou and Muramatsu 2003; Reddy, Manorama and Reddy, 2003). Titania is particularly important photocatalyst due to its strong oxidizing power, non–toxicity and long–term photostability (Tayade, et al., 2007; Reddy, Manorama and Reddy, 2003). The photocatalytic activity of titania depends on its phase structure, crystallite size, specific surface area, pore structure and thermal stability (Tayade, et al., 2007; Reddy, Manorama and Reddy, 2003).

Titania exists in three different crystalline phases: rutile, anatase and brookite, among which rutile is a thermodynamic stable state, while the latter two phases are metastable (Tayade, et al., 2007; Reddy, Manorama and Reddy, 2003; Li, et al., 2009). Anatase polymorph is generally considered to be the most photacatalitically active (Tayade, et al., 2007; Li, et al., 2009). Moreover, anatase with higher crystallinity is preferred for photocatalysis, since higher crystallinity means fewer defects for the recombination of photogenerated electrons and holes (Li, et al., 2009). Therefore, in order to increase crystallinity and, consequently, photocatalytic activity, calcination is often employed. On the other hand, thermodynamically metastable anatase phase easily transforms into the stable rutile phase when titania is calcined at high temperature (Li, et al., 2009). Furthermore, transformation to the rutile phase is usually accompanied with a severe decrease in specific surface area of photocatalyst, which usually results in a decrease in photocatalytic activity (Li, et al., 2009).

A wide variety of methods have been explored for the synthesis of titania nano particles (Sugimoto, Zhou and Muramatsu, 2003). The sol–gel process is generally the most popular method for preparing nanosized metal oxides (Reddy, Manorama and Reddy, 2003). As a titanium precursor for sol–gel process, titanium alkoxides are most often used (Jung, et al., 1999). However, depending on the molecular structure of the alkoxide precursor, sol–gel process parameters (e.g. hydrolysis method) and thermal treatment, different crystalline phases having various properties can be produced (Reddy, Manorama and Reddy, 2003). In order to prepare anatase nanoparticles and retain the size and morphology, low processing temperatures are of utmost importance. Therefore, although its preparation has been intensively investigated, controlled synthesis of nanosized titania with aimed properties remains a challenging task for material scientists.

Here we present a sol–gel method for producing pure anatase nanoparticles from titanium *n*–butoxide. Special attention has been paid to thermal evolution process in order to achieve anatase with small crystallite size and high specific surface area. Methylene blue, a cationic dye widely used in paper colouring, textile dyeing and coating for paper stock has been used as model industrial pollutant for the preliminary assessment of prepared catalyst photocatalytic activity.

2. Material and methods

Titanium *n*–butoxide ($Ti(O^nBu)_4$, 98 %, Alfa Aesar, Germany) was added to *i*–propanol (C_3H_7OH, 99 %, Kemika, Croatia) using a syringe in a closed reactor. Mixture was stirred for 24 h at room temperature to minimize exposure to humidity and no precipitation was observed. The

clear sol was poured into large Petri dish in order to maximize exposure to air moisture and kept at room temperature until gelation. Drying of the sample for five more days at room temperature enabled the evaporation of solvent. The obtained sample was subsequently grinded to fine powder and stored.

The thermal evolution of gel was characterized with DTA–TGA thermal analysis using Netsch STA 409C. For the thermal analysis ~50 mg of material were placed in Pt crucibles and heated at a rate of 10 °Cmin^{-1} in a synthetic air flow of 30 cm^{3}min^{-1}. α–alumina was used as a reference.

IR spectra were acquired using the Fourier transform infrared spectrometer Bruker Vertex 70 in ATR (attenuated total reflectance) mode. The samples were pressed on a diamond and the absorbance data were collected between 400 and 4000 cm^{-1} with spectral resolution of 1 cm^{-1} and 64 scans.

The powder X–ray diffraction (XRD) was accomplished using Shimadzu diffractometer XRD 6000 with CuKα radiation. Data were collected between 10–80 °2θ, in a step scan mode with steps of 0.02° and counting time of 0.6 s. The average crystallite size of anatase was calculated from the broadening of (100) diffraction peak using Scherrer´s equation: $D=k\lambda/(B\cos\theta)$, where *D* is the average crystallite diameter, *k* is Scherrer's constant (0.94), λ is the X–ray wavelength (0.15418 nm), *B* is full width at the half height of (100) diffraction peak corrected for instrumental broadening and θ is the diffraction angle.

Surface area was determined by Brunauer–Emmet–Teller (BET) N_2 gas adsorption–desorption isotherms obtained at -196 °C on a Micromeritics ASAP–2000 equipment. Samples were previously degassed at 100 °C under a dynamic vacuum of 1.3 × 10^{-2} Pa. Pore size distributions were calculated from the desorption isotherms by the Barrett-Joyner-Halenda (BJH) model.

The UV–Vis spectrum of the prepared sample was obtained using DRS (Shimadzu UV–3101PC) equipped with an integrating sphere. The spectra were recorded at room temperature in the wavelength range of 200–800 nm. $BaSO_4$ was used as a reference. The diffuse reflectance spectra were transformed by performing a Kubelka–Munk transformation of the measured reflectance according to: $F(R)=(1-R)^2/(2R)$, where F(R) is proportional to the extinction coefficient (α) and R is the reflectance of the "infinitely thick" layer of the solid. (Lopez and Gomez, 2012). The bandgap energy, *Eg*, was estimated by plotting modified Kubelka-Munk function, $(F(R)h\nu)^n$, vs. photon energy (hν), the so–called Tauc's plot, followed by extrapolation the linear region of high slope region onto the energy axis. In modified Kubelka–Munk function *h* is Planck's constant (4.13566733 eVs) and ν is frequency, quotient of light velocity (c=299792458 ms^{-1}) and wavelength, (λ/m). The exponent *n* is associated with electronic transition in the course of optical absorption process and is theoretically equal to ½ and 2 for indirect and direct allowed transitions, respectively (Lopez and Gomez, 2012). Direct transition occurs when electron can shift from the lowest energy state in the conduction band to the highest energy state in the valence band emitting a photon without a change of crystal momentum while indirect transition occurs with a change in crystal momentum and the process involves absorption of phonon with momentum enabling overall conservation of crystal momentum.

The photocatalytic activity of nanocrystalline anatase was determined by studying the degradation of methylene blue as a model compound. As photocatalytic reactor, a borosilicate cylindrical glass vessel with 100 mm diameter and 120 mm height was used. A quartz glass tube with a lamp inside was placed axially in the center of the vessel. Pen Ray lamp (UVP Products Cat. No. 90–0012–01), with radiation wavelength 254 nm and emission intensity of 2 mWcm^{-2}, was used as UV source. Prior to placing in the reactor, a 500 cm^3 of 10 ppm methylene blue aqueous solution containing 500 mg of catalyst was ultrasonicated for 30 min. After placing in reactor the mixture was stirred using magnetic stirrer operating at 300 rpm to maintain homogeneous reaction mixture and irradiated. The photodegradation experiments were carried out at room temperature (25 °C). Aliquots of 5 cm^3 were withdrawn from the mixture by a syringe at regular intervals of 30 min. First aliquot was withdrawn from the mixture before the commencement of irradiation. The photo–degradation was monitored with a UV–Vis Shimadzu UV–3101PC spectrophotometer. Spectra were acquired and intensity of main methylene blue absorption band at ~660 nm measured. The discoloration ratio was calculated as ratio between absorbance after measurement interval and absorbance prior to irradiation. The degradation of a substance was depicted as discoloration ratio

as a function of the irradiation time. A study of photocatalytic activity of commercial titania sample Degussa P90 was also carried out.

3. Results and discussion

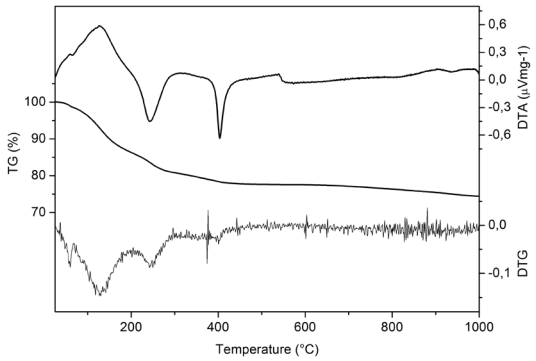

Figure 1. DTA, TGA and DTG curve of dried gel obtained with heating rate of 10 °Cmin^{-1} in air.

In order to gain insight into gel thermal evolution, a differential thermal and thermo-gravimetric analysis of dried gel has been made (Fig. 1). Thermal behavior of dried gel was studied in synthetic air up to 1000 °C. Five processes could be detected on the basis of DTA, TGA and DTG curves: Endothermic processes accompanied with the mass losses in a range between room temperature and 200 °C; two exothermic processes in a range between 200 and 300 °C and 300 and 500 °C, also accompanied with the mass loss; exothermal process starting from 540 °C and continuous mass loss takes place in the interval of 600–1000 °C. The mass loss seems to be constant until the end of measurement, indicating that a pure titania has not been obtained even at 1000 °C. The DTA and TGA curves have been interpreted on the basis of FTIR and XRD scans of gel samples quenched from various temperatures (Figs. 2 and 3).

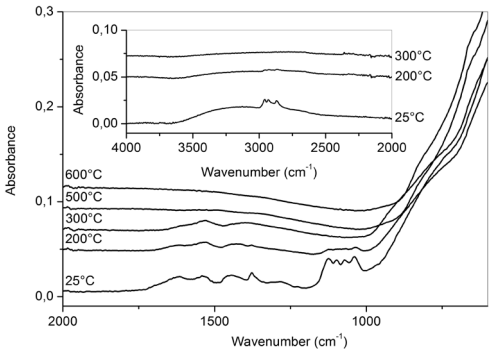

Figure 2. FTIR spectra of gel samples quenched from various temperatures. Spectra are shifted vertically for visualization purposes. Inset: Spectra of samples quenched from various temperatures in the wavenumber interval between 4000 and 2000 cm^{-1}.

Figure 2 shows the FTIR spectrum of dried gel (25 °C) as well as FTIR spectra of samples quenched from various temperatures. FTIR spectrum of dried gel shows a set of three vibrations at 2,960, 2,930 and 2,870 cm^{-1} corresponding to alkoxide asymmetric stretching vibration modes of –CH_3 and –CH_2– groups and symmetric stretching vibration mode –CH_3 groups, respectively (Bahloul, et al., 2011; García–Beniume, Espitia–Cabrera and Contreras–García, 2010; Velasco, et al., 1999). Bands at 1,445 and 1,375 cm^{-1} are related to –CH_3– and –CH_2– deformation vibration of the alkoxide group (Bahloul, et al., 2011; García–Beniume, Espitia–Cabrera and Contreras–García, 2010; Velasco, et al., 1999). The Ti–O–C stretching can be observed at 1,125 cm^{-1} (Bahloul, et al., 2011; Velasco, et al., 1999) while the absorption bands at 1080, 1070 and 1040 cm^{-1} could be attributed to the –C–O– vibration of alkoxide groups linked to Ti (Bahloul, et al., 2011; Velasco, et al., 1999). The broad band between 3700–2500 cm^{-1} centered at ~3125 cm^{-1} (Fig. 2, inset) is due to the stretching vibration of the hydroxyl groups of adsorbed water and rigidly bound water in the form of hydroxyls ions (Ti–OH groups) (Bahloul, et al., 2011; García–Beniume, Espitia–Cabrera and Contreras–García, 2010; Velasco, et al., 1999). The presence of adsorbed water is confirmed by the occurrence of –OH bending vibration of H_2O at 1625 cm^{-1} (Bahloul, et al., 2011; García–Beniume, Espitia–Cabrera and Contreras–García, 2010; Velasco, et al., 1999). Therefore, FTIR scan has shown that the dried gel is comprised of hidroxy groups and non-hydrolyzed butoxy groups, both bonded to titanium.

Compared with the dried gel, spectrum of sample quenched from 200 °C show reduced intensities of vibrations due to a $–CH_3–$ and $–CH_2–$ groups. The intensity of broad band between 3600 and 3000 cm^{-1}, corresponding to water vibrations, has also decreased (Fig. 2, inset). Therefore, first process characterized by endothermic peak and corresponding mass loss is the consequence of the evolution of adsorbed butanol and water. Thermal treatment of the sample from 300 °C yields with the disappearance of butoxide absorption bands in range between 1000 and 1200 cm^{-1}. So, second process is release and burning of butoxide groups. Sample quenched from 500 and 600 °C shows no vibration modes except broad envelope between 400 cm^{-1} and 800 cm^{-1}, generally considered as being due to the presence of Ti–O–Ti network (Krunks, et al., 2005; Chen and Mao, 2007; Velasco, et al., 1999), evidencing the condensation reactions and thus the building of the inorganic network (Bahloul, et al., 2011). FTIR spectra provide no information on other processes. It could be supposed that exothermal peak centered at ~404 °C is due to anatase crystallization while wide peak starting from 540 °C is due to transformation of anatase to rutile. Finally continuous mass loss in the interval of 600–1000 °C seems to correspond to the combustion of carbonaceous species formed due to incomplete oxidation of organics. In order to confirm those assumptions, XRD patterns of samples quenched from various temperatures were acquired.

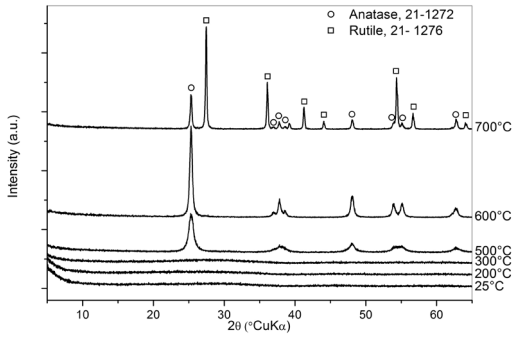

Figure 3. Powder XRD patterns of gel samples quenched from various temperatures. Spectra are shifted vertically for visualization purposes.

The structural changes accompanying thermal treatment of the gel over the temperature range of 25–700 °C are summarized in Figure 3 where diffraction patterns are presented. The powder X–ray diffraction pattern of dried gel (25 °C) show few low–intensity broad humps, indicating that the prepared gel is amorphous. After thermal treatment at 300 °C the sample was still amorphous. Broad peaks indicating fine crystallinity could be observed for the sample thermally treated at 400 °C, while thermal treatment of sample at 500 °C leads to the appearance of well–defined diffraction peaks corresponding to those of anatase (ICDD–PDF No. 21–1272). Thermal treatment at 600 °C yields with small improvement of crystallinity indicating grain growth. However, at this temperature a partial phase transformation from anatase to rutile (ICDD–PDF No. 21–1276) was observed.

Therefore, DTA and DTG peaks are attributed as follows: endothermic processes and mass loss in room temperature to 200 °C range is attributed to the elimination of adsorbed water and butanol on the grain surface and inside composite particles (You and Hsu, 2010). Decomposition and elimination of butoxy groups occurs in all samples between 200 and 300 °C (Madarasz, et al., 2009). Exothermal process centered at 404 °C can safely be attributed to the crystallization of anatase. The origin of the weight loss in the same temperature interval is not quite clear. Some authors attribute mass loss in this temperature interval to dehydroxylation of Ti–OH groups formed in the course of hydrolysis (Chang, et al., 2002; Cernea, et al., 2007). On the other hand, in present investigation no indication for the presence of –OH groups in this temperature interval was found. Exothermal process starting from 540 °C is a consequence of transformation of anatase to rutile. Finally, weight loss above 600 °C could be attributed to the oxidation of char and tar remained within powder grains. According to Madarasz et al. (Madarasz, et al., 2009) a slow permanent oxidation of tarred components, accompanied by the release of carbon dioxide, starts above 500 °C and could proceed up to high temperatures. The residues of sample quenched from 500 °C are still grayish colored. It seems that hindered butoxide degradation leave carbonaceous residual resistant to oxidation until higher temperatures are reached (Madarasz, et al., 2009). Thermal treatment at higher temperatures brings about slow oxidation of char and tar remained within powder grains.

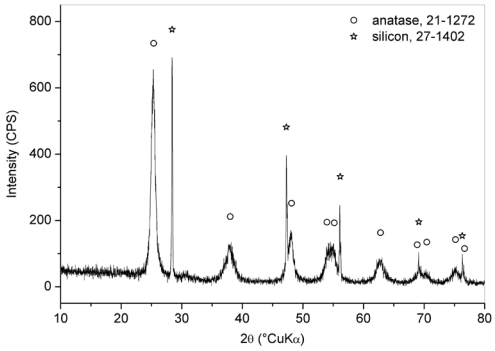

Figure 4. Powder XRD pattern of sample thermally treated at temperature of 350 °C for 2 h. Silicon (ICDD PDF No. 27–1402) has been added as internal standard.

On the basis of DTA/TGA and XRD analysis the gel was thermally treated at 350 °C. Thermal treatment of gel at 350 °C for 2 h leads to the appearance of well–defined diffraction anatase (JCPDS–PDF No. 21–1272) peaks (Fig. 4). Broad diffraction peaks point out to the nanocrystalline character of anatase. The average crystallite size of anatase has been calculated using Scherrer's equation and yields 13.2±0.2 nm.

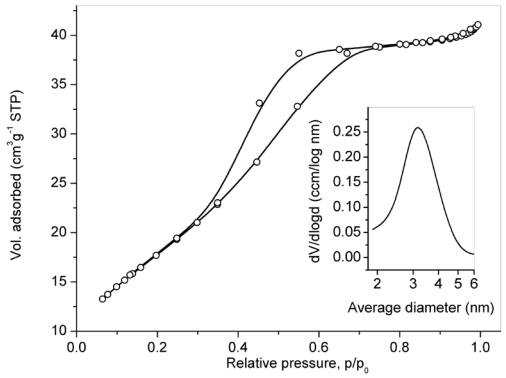

Figure 5. N_2 adsorption – desorption isotherms of sample thermally treated at 350 ° C for 2h. Inset: Pore size distribution.

Figure 5 presents the nitrogen adsorption/desorption isotherm of the sample thermally treated at 350 °C for 2 h and the inset shows the pore size distribution derived therefrom. The isotherm exhibit a type IV isotherm with a H2 hysteresis loops indicating the presence of mesopores (Jitputti, et al., 2007; Huang, et al., 2005). The BET surface area of sample has been calculated to be 65.48 m^2g^{-1}. The BJH analysis for the sample yields a peak at the approximate pore radius of 3.2 nm (Fig. 5, inset) and the pore volume has been calculated to be 4.6 nm. The fact that the N_2–determined surface area (S_{BET} = 65.48 m^2g^{-1}) is much less than the geometric surface area (S_G = 117.15 m^2g^{-1}), calculated assuming spherical particles and using formula: $S_G=6/(D\times\rho)$ (Zaki, et al., 2010), where *D* is average crystallite size calculated through Scherrer's equation and ρ is average anatase density (ρ = 3.93 gcm^{-3}), may imply considerable aggregation of particles.

In the past H2 loop was attributed to a difference in mechanism between condensation and evaporation processes occurring in pores with narrow necks and wide bodies (often referred to as 'ink bottle' pores), but now is recognized that this provides an over-simplified picture (Sing, et al., 1985). Nowadays, hysteresis loop of this type is believed to be associated with pores generated by agglomerates or compacts of particles of non-uniform size and arrangement (Zaki, et al., 2010; Bajunajdad, et al., 2006).

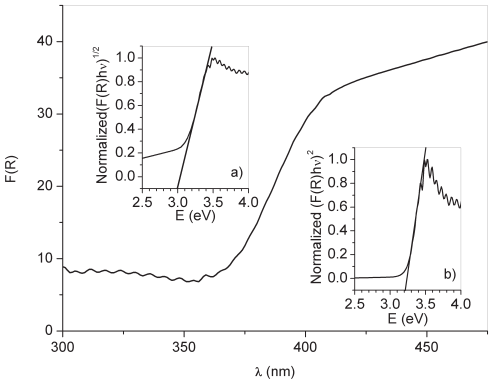

Figure 6. UV–Vis diffuse reflectance spectrum of the sample thermally treated at 350 °C for 2 h. Insets: Modifyed Kubelka-Munk function for a) indirect transition, n=1/2 and b) direct transition n=2.

Figure 6 presents UV–Vis F(R) spectra (Kubelka–Munk function) of the sample thermally treated at 350 °C for 2 h. Spectrum shows strong absorbance in UV region and fair reflectance in Vis region. Modified F(R) functions for direct and indirect allowed transitions have been plotted against E. Anatase interband transitions are generally taken as indirect (Coronado, et al., 2013; López-Granada, et al., 2013), however other factors like crystallite size or the presence of dopants can modify the type of transition making the direct transition more appropriate (Coronado, et al., 2013; Reddy, Manorama and Reddy, 2003) and somewhat conflincting reports are found in

literature (Coronado, et al., 2013). These two different kinds of transitions can be distinguished by the energy dependence of the corresponding absorption edge. To establish the type of the bandgap transitions which occur in the prepared sample $(F(R)h\nu)^{1/2}$ and $(F(R)h\nu)^2$, for the indirect allowed and direct allowed transitions, respectively, were fitted against E and the linear relationships have been obtained for both cases. Therefore, the bandgap of the sample was obtained from the extrapolation linear part of the curve onto the energy axis in plot for both indirect (Fig. 6a) and direct (Fig. 6b) transition. As can be seen, in the indirect transition the extrapolation yields an *Eg* value of 3.0 eV, while for the direct transition *Eg* equals 3.2 eV.

For the anatase there have been reported values in the literature from 2.86 to 3.34 eV, the differences being attributed to variations in the stoichiometric of the synthesis, the impurities content, the crystalline size and the type of electronic transition (Valencia, Miguel Marín and Restrepo, 2010). Thus, although the bandgap obtained for direct transition is close to the literature value for bandgap of bulk anatase, *Eg* ≈3.23 eV (382 nm) (Kim, et al., 2008) neither the bandgap estimated for indirect transition seems unrealistic. Therefore, regardless of the nano character of the prepared sol-gel derived anatase it was concluded that there was no evidence that direct transition is more appropriate.

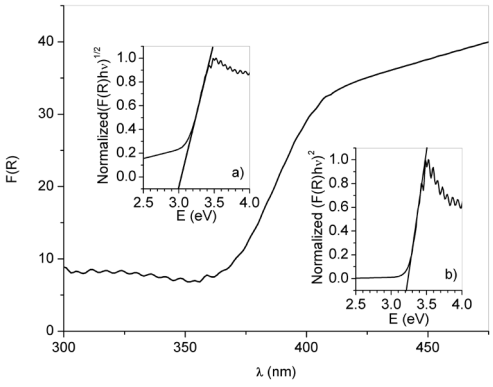

*Figure. 7. Photocatalytic discoloration of MB over TiO_2 catalyst and commercial titania at room temperature, pH = 7, initial MB concentration = 10 ppm, catalyst concentration = 1 gdm-**3.** The lines are introduced as a guideline for the eye.*

The assessment of prepared catalyst photocatalytic activity was obtained through degradation process of 10 ppm aqueous solution of MB in the presence of 1 gL^{-1} of catalyst. In the spectra of MB recorded after illumination with UV light with respect to time two peaks were initially observed at 664 and 612 nm, which merged at higher irradiation times and the maximum absorbance was finally observed at around 636 nm. Still, absorbance change at λ_{max} versus irradiation time was used to test the photocatalytic activity of titania qualitatively. The reduction of maximal absorbance was recorded with respect to time elapsed from the beginning of irradiation of UV light. The photocatalytic activity of the prepared catalyst has been presented as discoloration ratio in dependence on irradiation time in Figure 7. The photocatalytic activity of commercial titania sample was tested under the same conditions for the purpose of comparison. The data clearly indicate that the MB discoloration ratio by prepared photocatalyst is much faster than that by commercial titania, which implies that photocatalytic activity of prepared sample is greater than reference. When commercial titania was used as photocatalyst, only 58 % MB could be discolored within 60 min irradiation, whereas 92 % MB discoloration ratio could be obtained in the same reaction time for prepared catalyst. With the prepared photocatalyst the 99 % degradation of dye took place within 150 min.

The data on photocatalyst properties gave no conclusive reason for its advantageous behavior in comparison with commercial titania. The factor of utmost importance for the photocatalytic activity is surface area providing better adsorption of dye and higher number of surface catalytic sites with less recombination of electron hole pairs, which is the rate–determining step in the photocatalytic degradation . The optimum band–gap also plays an important role in the photocatalytic activity of anatase. Electron hole pair generation is dependent on the bandgap of TiO_2 and the increase of the bandgap is beneficial for electron hole pair generation. Finally, microstructure of the photocatalyst was reported to play important role for the dye degradation (Liu, Liu and Zhang, 2008). As it was shown earlier, specific surface area of prepared anatase photocatalyst shows no superiority with respect to commercial titania, the bandgap is the same as bulk anatase and no special microstructural features of prepared photocatalyst have been noted. On the other hand, a huge turbidity of commercial titania suspension has been observed, pointing out to agglomeration of primary particles, while the prepared photocatalyst suspension

was quite clear. It could be argued that ultrasonic agitation was far more successful in breaking of the prepared photocatalyst agglomerates than for commercial titania. One of the consequences of such development is that in given experimental conditions specific surface area of prepared photocatalyst is higher in comparison with agglomerated commercial titania particles. On the other hand, it is quite clear that the impaired suspension transparency presents obstacle to particles light absorption and consequently causes reduced oxidation. It is quite plausible that this effect has greater influence on photocatalytic properties. So, it is reasonable to say that advantageous oxidation behavior of prepared photocatalyst in given experimental conditions is caused by enhanced suspension transparency and increased specific surface area due to better particles dispersion.

4. Conclusion

Titania gel has been synthesized via sol–gel method using titanium n–butoxide as a precursor and slow hydrolysis with air moisture.

The amorphous gel was comprised of hidroxy groups and non-hydrolyzed butoxy groups bonded to titanium. The thermal evolution of gel is consisted of five steps: elimination of adsorbed water and butanol in room temperature to 200 °C range, decomposition and elimination of butoxy groups between 200 and 300 °C. The crystallization of anatase centered at 404 °C, transformation to rutile starting from 540 °C and oxidation of char and tar above 600 °C.

Thermal treatment of gel at 350 °C for 2 h yields with pure nanocrystalline anatase. The average crystallite size, specific surface area and bandgap of the prepared anatase have been calculated to be 13.2±0.2 nm, 65.48 m^2g^{-1} and 3.2 eV, respectively.

The assessment of prepared photocatalyst activity was obtained through degradation process of methylene blue under UV light and the 99 % degradation of dye took place within 150 min.

Acknowledgements

The support of University of Zagreb is gratefully acknowledged.

References

1. Bahloul, W., Bounor–Legare, V., Seytre, G., Cassagnau, P., 2011. Influence of a non–polar medium (alkane and molten polypropylene) on the titanium n–butoxide hydrolysis–condensation reactions. Journal of Sol–Gel Science and Technology, 57, p.86.
2. Bajunajdad, A., Zaki, M. I., Eastoe, J., Pasupulety, L., 2006. Characterization of *nano*-cerias as synthesized in microemulsions by N_2 sorptiometry and electron microscopy. Journal of Colloid and Interface Science, 302, p.501.
3. Cernea, M., Valsangiacom, C., Trusca, R., Vasiliu, F., 2007. Synthesis of iron–doped anatase –TiO2 powders by a particulate sol–gel route. Journal of Optoelectronics and Advanced Materials, 9, p.2648.
4. Chang, T. C., Wang, Y. T., Hong, Y. S., Chiu, Y. S., 2002. Effects of inorganic components on the structure and thermo–oxidative degradation of PMMA modifyed metal alkoxide–EAA complex. Thermochimica Acta, 390, p.93.
5. Chen, X., Mao, S. S., 2007. Titanium dioxide nanomaterials: synthesis, properties, modifications and applications. Chemical Review, 107, p.2891.
6. Coronado, J. M., Fresno, F., Hernandez-Alonso, M., Porteza, R., 2013. Design of advanced photocatalytical materials for energy and environmental applications. Springer-Verlag, London, p.96.
7. Dogan, M., Alkan, M., 2003. Adsorption kinetics of methyl violet onto perlite. Chemosphere, 50(4), p.517.
8. García–Benjume, M. L., Espitia–Cabrera, M. I., Contreras–García, M. E., 2010. The effect of synthesis parameters on the production of titania nanostructured spherical aggregates. Journal of Ceramic Processing Research, 11, p.198.

9. Huang, D., Luo, G., Yang, L., Wang, Y., 2005. Synthesis of mesoporous TiO_2 materials with high specific area using inorganic acids as catalysts. China Particuology, 3, p.176.

10. Jitputti, J., Pavasupree, S., Suzuki, Y., Yoshikawa, S., 2007. Synthesis and photocatalytic activity for water–splitting reaction of nanocrystalline mesoporous titania prepared by hydrothermal method. Journal of Solid State Chemistry, 180, p.1743.

11. Jung, M. W., Oh, H. J., Yang, J. C., Shul, Y. G., 1999. Structural investigation of the hydrolysis-condensation process of modified titanium isopropoxide. Bulletin of the Korean Chemical Society, 20, p.1394.

12. Kim, G.-M., Lee, S.-M., Michler, G. H., Roggendorf, H., Gosele, U., Knez, M., 2008. Nanostructured pure anatase titania tubes replicated from electrospun polymer fiber templates by atomic layer deposition. Chemistry of Materials, 20, p.3085.

13. Krunks, M., Oja, I., Tõnsuaadu, K., Es–Souni, M., Gruselle M., Niinistö, L., 2005. Thermoanalytical study of acetylacetonate–modifyed titanium (IV) isopropioxide as isopropoxide as precursor for TiO_2 films. Journal of Thermal Analysis and Calorimetry, 80, p.483.

14. Lachheb, H., Puzenat, F., Houas, A., Ksibi, M., Elaloui, F., Guillard, C., Herrmann, J., 2002.

15. Photocatalytic degradation of various types of dyes (Alizarin S, Crocein Orange G, Methyl Red, Congo Red, Methylene Blue) in water by UV-irradiated titania. Applied Catalysis B: Environmental, 39, p.75.

16. Li, Y., Sun, X., Li, H., Wang, S., Wei, Y., 2009. Preparation of anatase TiO_2 nanoparticles with high thermal stability and specific surface area by alcohothermal method. Powder Technology, 194, p.149.

17. Liu, Y., Liu, C.–Y., Zhang, Z. –Y., 2008. Effects of carboxylic acids on the microstructure and performance of titania nanocrystals. Chemical Engineering Journal, 138, p.596.

18. Lopez, R., Gomez, R., 2012. Band–gap energy estimation from diffuse reflectance measurements on sol–gel and commercial TiO2: a comparative study. Journal of Sol–Gel Science and Technology, 61, p.1.

19. López-Granada, G., Barceinas-Sánchez, J. D. O., López, R., Gómez, R., 2013. High temperature stability of anatase in titania–alumina semiconductors with enhanced photodegradation of 2,4-dichlorophenoxyacetic acid. Journal of Hazardous Materials, 263, p.84.

20. Madarasz, J., Braileanu, A., Crisan, M., Pokol, G., 2009. Comprehensive evolved gas analysis (EGA) of amorphous precursors for S–doped titania by in situ TG–FTIR and TG/DTA–MS in air: Part 2. Precursor from thiourea and titanium(IV)–n–butoxide. Journal of Analytical and Applied Pyrolysis, 85, p.549.

21. Mall, I. D., Srivastava, V. C., Agarwal, N. K., 2006. Removal of Orange-G and Methyl Violet dyes by adsorption onto bagasse fly ash-Kinetic study and equilibrium isotherm analyses. Dyes and Pigments, 69(3), p.210.

22. Pokhrel, D., Viraraghavan, T., 2004. Treatment of pulp and paper mill wastewater—a review. Science of the Total Environment, 333, p.37.

23. Reddy, K. M., Manorama, S. V., Reddy, A. R., 2003. Bandgap studies on anatase titanium dioxide nanoparticles. Materials Chemistry and Physics, 78, p.239.

24. Sing, K. S. W., Everett, D. H., Haul, R. A. W., Moscou, L., Pierotti, R. A., Rouquerol, J., Siemieniewska, T., 1985. International union of pure and applied chemistry, Physical chemistry division, Commission on colloid and surface chemistry including catalysis, reporting physisorption data for gas/solid systems with special reference to the determination of surface area and porosity. Pure and Applied Chemistry, 57, p.603.

25. Sivalingam, G., Nagaveni, K., Hegde, M., Madras, G., 2003. Photocatalytic degradation of various dyes by combustion synthesized nano anatase TiO2. Applied Catalysis B: Environmental, 45, p.23.

26. Sugimoto, T., Zhou, X., Muramatsu, A., 2003. Synthesis of uniform anatase TiO2 nanoparticles by gel–sol method 3. Formation process and size control. Journal of Colloid and Interface Science, 259, p.43.

27. Tayade, R. J., Surolia, P. K., Kulkarni, R. G., Jasra, R. V., 2007. Photocatalytic degradation of dyes and organic contaminants in water using nanocrystalline anatase and rutile TiO_2. Science and Technology of Advanced Materials, 8, p.455.

28. Valencia, S., Miguel Marín, J., Restrepo, G., 2010. Study of the bandgap of synthesized titanium dioxide nanoparticles using the sol-gel method and a hydrothermal treatment. The Open Materials Science Journal, 4, p.9.

29. Velasco, M. J., Rubio, F., Rubio, J., Oteo, J.L., 1999. DSC and FT–IR analysis of the drying process of titanium alkoxide derived precipitates. Thermochimica Acta, 326, p.91.

30. You, J.–H., Hsu, K.–Y., 2010. Influence of chelating agent and reaction time on the swelling process for preparation of porous TiO2 particles. Journal of the European Ceramic Society, 30, p.1307.

31. Zaki, M. I., Mekhemer, G. A. H., Fouad, N. E., Jagadale, T. C., Ogale, S. B., 2010. Surface texture and specific adsorption sites of sol–gel synthesized anatase TiO_2 nanoparticles. Materials Research Bulletin, 45, p.1470.